Title

Post-irradiation characterization of a high burnup mixed oxide fuel rod with minor actinides

Authors

Frazer, D

Cappia, F

Harp, JM

et al.

Publication Date

2022-04-01

DOI

10.1016/j.jnucmat.2022.153545

Post-Irradiation Characterization of a high burnup Mixed Oxide Fuel Rod with Minor Actinides

D. Frazer[1,2*], F. Cappia[2], J.M. Harp[2§], P.G. Medvedev[2], K.J McClellan[3], S.L. Voit[3], J. Giglio[2], D. Jädernäs[2§§], P. Hosemann[1,4]

1 University of California at Berkeley, Nuclear Engineering Department, 94720, CA, USA

2 Advanced Characterization and PIE, Idaho National Laboratory, 2525 Fremont Ave, Idaho Falls, ID USA

[3] Material Science and Technology Division, Los Alamos National Laboratory, Los Alamos, NM, USA

[4] Material Science Division, Lawrence Berkeley National Laboratory, Berkeley, CA, United States

§Currently at Oak Ridge National Laboratory

§§ Currently at Studsvik A.B.

[*]David.Frazer@inl.gov

Abstract

The Advanced Fuels Campaign performed a series of irradiation tests of minor actinide-bearing mixed oxide fuel (MA-MOX), the so-called AFC-2C&D experiments, to investigate the transmutation of long-lived transuranic actinide isotopes contained in spent nuclear fuel via fast reactor technology at burnups exceeding 10 % fission of initial metallic atoms. This manuscript reports the test results derived from one of the five MA-MOX rodlets taken to higher burnup in the AFC-2D irradiation. This includes both non-destructive investigations, such as gamma and neutron spectrometry, and destructive investigations, such as fission gas release, ceramography, and chemical burnup analysis. In addition, the microstructure of the fuel was investigated using advanced electron microscopy techniques including electron backscatter diffraction (EBSD) and transmission electron microscopy (TEM). It was observed with EBSD that the pellet had subdivision of the grains and the TEM observed migration of cladding material into the 5 metal precipitates in the fuel which could have been from the higher than desired oxygen/metal ratio. The TEM also showed an enrichment of Cr in fuel clad chemical interaction (FCCI) layer.

Keywords: Mixed Oxide fuel, post irradiation analysis, advanced electron microscope characterization, minor actinides

Introduction

The once through open fuel cycle of current light water nuclear reactors produces spent fuel that requires very long disposal times lasting 100,000s of years [1-4]. The long-lived minor actinides (MA) such as americium and neptunium are the primary cause of the long-term radiotoxicity of the spent fuel, requiring such long disposal times [1-4]. The MA are capable of undergoing fission and can be transmuted in current light water reactors [4-6], fast reactors [7-9], fusions

reactors [10-12] or accelerator driven systems [13-15] after recovery during fuel reprocessing. The transmutation of the MA can reduce the required disposal time of spent nuclear fuel to as short as 500-1000 years, as well as decreasing the volume of nuclear waste through recycling [4-19]. The AFC-2C&D irradiation tests (low and high burnup, respectively) investigated the viability of transmutation of minor actinide-bearing mixed oxide fuels (MA-MOX) in the Advanced Test Reactor (ATR) at Idaho National Laboratory (INL) by adapting the irradiation conditions to mimic a fast spectrum by utilizing a Cd shroud to transmute the MA within the fuel [20, 21]. A fast spectrum is preferred for transmutation because the fission-to-capture ratio of fast neutrons is significantly larger than for thermal neutron [22]. That is, a fast neutron has a higher probability to induce a fission of the actinides, and hence transmute them into fission products, than the probability that it would be captured by the actinide nucleus and convert it to a nucleus of an even heavier element (what is more likely to happen with slow, thermal neutrons) [22]. There are two genres of fuel employed when burning MA in reactors: homogenous and heterogeneous. In homogenous designs a small amount of MA is mixed in a MOX or UO_2 fuel evenly distributed throughout the pellet and core. In the heterogeneous design MA fuel pins with up to 20 % MA are fabricated and burned in the reactor. The fuel in this irradiation campaigns would correspond to homogeneous design. This work presents the non-destructive, destructive and advanced electron microscopy investigations of an AFC-2D rodlet of MA-MOX $(U_{0.75}Pu_{0.20}Am_{0.03}Np_{0.02})O_{1.986}$ fuel clad in HT-9 that was irradiated to 10.6 % fissions initial metal atom (FIMA) in the ATR [23].

Substantial irradiation tests have been performed on MOX in different countries [24-29] (see for example the reviews in [30-32]) with burnup exceeding 20% FIMA [33, 34]. The experience with MA-MOX fuels is more limited [35-38]. Initial tests in the Japanese JOYO reactor were focused on the understanding of Am and Np redistribution during the first hours of irradiation in order to dismiss the penalty in thermal conductivity and melting point due to addition of the minor actinides as a safety concern [39]. Tests to medium burnup (i.e., between 4.5 and 6.5 % FIMA) have been conducted in the SUPERFACT program, showing that the performance was satisfactory and PIE results were similar to what obtained for standard MOX pins [30, 33, 40-44]. Extension to high burnup above 10% FIMA has been hindered by the early shut down of SFR, and the AFC-2D irradiation test were targeted to fill this gap.

Experimental

The full production details and characterization of MA-MOX fuel pellets can be found in the following [45]. The fabrication of the pellets begins with a blending of oxide powders of uranium, plutonium, neptunium, and americium. The milling of the powders is preceded by the addition of polyethylene glycol which is used as a lubricant for pressing and a binder for the green pellets [45]. This binder was removed in a low temperature furnace before the high temperature sintering of the pellets. The initial sintering of the pellets was performed under conditions resulting in a stoichiometric actinide. After the size of the pellets was verified and any grinding that needed to occur was completed the stoichiometry was adjusted by holding the pellets for 6 hours at 1350 °C with dry argon gas flowing through the furnace. The final

stoichiometry was measured to 1.986 using the standard thermogravimetric technique. In addition, the pellets had geometric density value between 9.473-10.3 g/cm^3.

The characteristic and irradiation conditions of the homogenous MA-MOX fuel examined in this work are reported in Table 1. The AFC-2D irradiation took place in ATR's east flux trap at INL. To mimic a fast spectrum from the ATR thermal spectrum the capsule was placed inside a Cd-shrouded basket to shield thermal neutrons creating a spectrum closer to a fast reactor spectrum [20, 46]. In this rodlet average Linear Heat Generation Rate (LHGR) and, consequently, the temperature of the fuel during irradiation was lower than typical fast reactors. The pellet peripheral temperature was calculated to be in the range 698-848 K, whereas typical peripheral temperature in fast reactor MOX can be as high as 1173 K [47]. A radial temperature profile can be seen in the supplementary material where a center-line temperature of 1787 K was calculated at middle of life.. The fuel was irradiated to an average burn-up of 10.6% FIMA or 112 GWd/tHM, which is the intend burn for lead rods in sodium fast reactor (SFR) fuel.

The non-destructive examinations included a visual examination, neutron radiography, gamma spectrometry and dimensional inspection. The visual examination of the rodlet was performed using photography through the hot cell window at the hot fuel examination facility (HFEF). The neutron radiography was performed with the HFEF neutron radiography reactor (NRAD) which is a 250 kW TRIGA reactor in the basement of HFEF [48]. The images for the neutron radiography were taken with cadmium filtered indium foils for the epithermal neutron imaging and dysprosium foils for the thermal neutron imaging. The HFEF Precision Gamma Scanner (PGS) was used to measure the axial profile of the major gamma emitters from the fuel fission products and cladding activation products. The dimensional inspection of the rodlet was performed with HFEF Plate and Rodlet checker. The rodlet was examined every 0.127 cm at 5 angles 45º apart. At each axial position, the average from all the orientation was performed to obtain the axial profile of the cladding diametral strain and associated standard error.

The destructive examination included fission gas release analysis, optical microscopy, analytical chemistry analysis for burnup and advanced electron microscopy. Optical microscopy was performed with a Leitz MM5RT metallograph on fuel cross sections to investigate the irradiation induced features in the fuel microstructure. The samples for optical microscope were prepared by sectioning the fuel rod with a low speed saw with a diamond coated wafer blade. Two samples were cut at the mid axial height in the active column and were then potted in epoxy and polished to a finish of 0.25 µm diamond suspension. One of these samples was further sub-sized into a "matchstick" geometry for further electron microscopy examination. The sample for electron microscopy was potted in an epoxy with 15 wt.% graphite to minimize the sample charging in the microscope. The sample was examined using a Quanta FEI FEG 3D scanning electron microscope/focused ion beam (SEM/FIB) both in electron microscope laboratory (EML) and irradiated materials characterization laboratory (IMCL) at INL. The SEM/FIB systems were used to extract TEM foils for subsequent TEM characterization at IMCL using the chemiSTEM on a FEI Titian microscope. The FIB extracted TEM foils were manufactured at the interface between the fuel and cladding material. In addition, SEM images and EBSD were acquired on the sample

to investigate the microstructure. The EBSD data was collected with an EDAX detector at 30 keV with a step size of 50 nm. The EBSD was performed in region of r/r_0 = 0.13-0.3

Samples of the fuel were sent to the Analytical Laboratory at INL for fuel chemical burnup analysis. The burnup is calculated from the results of mass spectrometry examination of dissolved fuel samples. In this analysis the samples were dissolved in 8M nitric acid kept near boiling for 24 hours. Aliquots of the original dissolution were diluted and sent through different inductively coupled plasma mass spectrometry devices (ICP-MS) to determine the isotopic composition of the major constituents and fission products. A "fission product monitor- residual heavy atom" [49, 50] technique was then used to evaluate the burn up of the fuel which was compared to simulated results.

Results

The results of the non-destructive PIE are presented in Figure 1 through Figure 3. The visual examination of the rodlet, seen in Figure 1A, indicates no signs of damage or failure from the irradiation. Some discoloration is visible in the area corresponding to the active fuel stack, which is a routine observation in the visual examinations of the rodlets. The results of the neutron radiography seen in Figure 1B and 1C show no formation of the central hole in any of the axial locations. While other rodlets in the irradiation did show the formation of a center void, the position of this rodlet in the AFC-2D capsule was at lower temperature [21, 23]. In addition, the sample was irradiated for 633 equivalent full power days and had a fission density of approximately $1.85*10^{21}$ fissions/cm^3. However, the image does show the fuel swelled during the irradiation which was expected. The active fuel stack length has increased by approximately 2% compared to the nominal stack length. The axial gamma spectrometry is displayed in Figure 2. The axial profile shows that Cs was migrating towards the end of the fuel column while the rest of the fission gamma ray emitting products (Ru, Eu, Ce,) did not redistribute axially. The gamma spectrometry suggests that the fuel was hot enough to cause the Cs and its compounds to become gaseous allowing it escape to the plenum and condense at cooler places in the rodlet. This migration occurred with both the Cs-137 which migrates mainly as Cs and with Cs-134 which can migrate as its parent nuclides, Xe-133 and Cs-133. The Cs-134 profile followed the Cs-137 in the fuel pellets. However, the Cs-134 content in the plenum of the AFC-2D rodlets is enhanced compared to the Cs-137 content. This is evidence of Xe-133 migration to the plenum prior to decay to Cs-133 and neutron capture to Cs-134. The plot of the diametral strain depicted in Figure 3 shows that all of the swelling was in the fuel region of the rodlet. Testing indicated that the fuel region of the rodlet had undergone a roughly 0.013 diametral strain. The results of fission gas release experiments can be seen in Table 2. The fission gas release was calculated at 56.79 % for Kr + Xe release.

In Figure 4 is a 50X montage of optical images of the fuel radial cross-section. It can be seen that the fuel is extensively cracked. However there is no formation of a central void as observed in other fast reactor fuel tests with MA-MOX [29, 36].

The SEM images in Figure 5a contain an overview of the match stick in the epoxy and the development of the high-burn structure (HBS) in the periphery, which is further highlighted by

the high magnification image shown in Figure 5b, where the typical HBS structure is visible: large pores with diameter of a few micron within the submicrometric grains, which give the pore surface a faceted appearance [51]. The EBSD map of the central part of the fuel is displayed in Figure 6. The EBSD map reveals that the fuel in the pellet center is has subdivided grains. It has been documented in a review of literature that UO_2 which has been irradiated at similar temperatures was affected in a similar manner [52]. A plot of the calculated temperature profile versus radius of the pellet can be seen in supplementary material. This plot was for the middle of life when the temperature peaked and shows the center of the pellet having a temperature of ~1787 K. This is lower than temperature need for center void formation which is 1973 K (agreeing with the optical and SEM investigations).

An image showing the FCCI layer is shown in Figure 7a, together with the qualitative energy dispersive spectroscopy (EDS) maps of the main components both on the fuel side (Figure 7b) and the cladding (Figure 7c and d) in addition to the corrosive fission products Cs and Te. The FCCI region presented the following characteristics: a dense layer with some interdiffusion between fuel and Fe with slight depletion in Cr, which had an approximate thickness of 15 µm. Moving towards the cladding interior, an azimuthal crack is visible, and the attack developed for further 50 µm continuously in the cladding. Lastly, penetration through intergranular attack continues up to ≈125 µm inside the cladding. The Cr content increases in the intergranular corroded areas, where it is associated with Cs and Te.

The location of the TEM foil extracted in the FCCI region is shown in Figure 8. The TEM foil confirmed that Fe and Cr have diffused into the fuel and mixed with the 5 metal precipitates which can be viewed in Figure 9. Figure 10 is an EDS map of the precipitates which shows that the Cr and Fe as well as the deposits of the 5 metal precipitates are not homogenously distributed in the large precipitate formations and that there is some segregation of the metals in the precipitates. In addition, the TEM EDS results indicate that FCCI has a large amount Cr and that Te has migrated to the FCCI through cracks in the material.

Discussion

The diametral strain for the fuel section of the rodlet was ~0.013 and was relatively uniform across the length of the fuel section. The diametral strain is believed to be cause by the swelling the in the fuel. This would suggest that there were uniform irradiation conditions along the length of the fuel section in the rodlet.

The visual examination showed no failures. The fuel and cladding material maintained structural integrity up to high burn up. This demonstrates that the MA-MOX fuel with HT-9 cladding is structurally sound under these irradiation conditions. The neutron radiography images also show that the fuel swelled during irradiation as anticipated, but there were no major failures in the fuel. Sodium fast reactor (SFR) MOX pins usually have a >80% fission gas release (FGR) at these burnups. This pin ran cold for SFR, which makes the 56% FGR is reasonable.

No restructuring occurred in the observed cross section with optical microscopy which left a fission gas bubble structure in place undisturbed by the rapid movement of porosity that occurs during restructuring. There are two unique fission gas bubble structures in the cross section of

the pellet. In the more central region the fuel was operating at a temperature that was hot enough to sweep the fission gas out of each grain to the grain boundaries. Further from the center of the cross section where the fuel was operating at lower temperatures, fission gas bubbles appear to be mostly intragranular and are only beginning to move towards the grain boundaries [23].

The SEM and optical microscopy confirm that there is no central void in this fuel after irradiation. The absence of a central void in the fuel would imply that the center of the pellet was below 1973 K [53, 54]. In addition, the lack of columnar grains in the optical microscopy and SEM would suggest the center of the pellet was below 1973 K which agrees with modeling of the fuel temperature that peaked at ~1773 K. The optical and SEM show that there was restructuring in the fuel with the formation of a HBS region at the periphery of the pellet. The formation of the HBS is well documented in UO_2 fuels when irradiated exceeding a local burnup of ≈50 GWd/tHM and where local irradiation temperature do not exceed 1273 K [52, 55-57]. Therefore, in LWR fuels the HBS structure starts developing at the pellet periphery, where temperature of ~ 773 K are achieved and the local burnup is higher than the pellet average due to the skin effect. In addition, the HBS has been seen in fast reactors as well [56, 58, 61-63]. Due to the pellet periphery temperature is slightly above the operating temperature of LWRs it is probable that the same driving forces and causes of the restructuring in UO_2 are present here. There is the same self-shielding effect that causes a larger number of the fissions in the fuel to occur in the periphery of the fuel. In examining the MOX-MA it would appear that the HBS is approximately ~400 µm thick and is that region of the pellet that does not exceed 1273 K from the plot in the supplementary material. The FCCI can be seen in the montage image of fuel. From the optical montage image it can be seen that the FCCI zone is 15 to 190 µm and that that there is significant wastage of the original cladding thickness. The reason for the azimuths difference in the fuel is not completely understood. Higher O/M ratios usually increase the FCCI observed in the irradiation.

The EBSD of near the center of the fuel clearly shows internal grain subdivision which has also been observed in light water reactor fuel [52, 59], which could suggest that this region of the fuel pellet was around 1273-1473 K during most of the irradiation, similar to light water reactor temperatures. The results of EBSD highlights the use of advanced electron microscope techniques to gain a deeper understanding of the irradiated fuel. There is still debate about the reasons for this subdivision in this region of the fuel because of the elevated temperature compared to the periphery of the pellet and HBS. It is believed that a polygonization process is reasonable for the grain subdivision [52, 59]. It can be seen in Figure 6a that there is a larger density of low angle grain boundaries (< 15°) in the area towards the center of the pellet. An increase in the number of low angle grain boundaries can be seen in [52] with irradiated UO_2.

The EDS maps from the TEM foils show that Fe and Cr from the HT9 cladding diffused into the MOX-MA fuel during the irradiation and precipitated into the 5 metal precipitates of the fuel. It is rather interesting that Fe and Cr are both in the large 5 metal precipitates while it appears that Fe is only in the smaller 5 metal precipitates. The diffusion of the Fe and Cr diffusion into the fuel and the fuel and fission products into the cladding can be seen at the macro scale in Figure 9 and agrees well with previous literature [24, 35, 60, 61].

The examination of the distribution of the metals in larger precipitates also indicated there was not a uniform distribution. Figure 10 illustrates that the Cr appears on the outer volume of the precipitates. This heterogeneous distribution can be seen in the other elements in the precipitates as well and been documented in literature [26, 62, 63]. In Figure 10 appears that Cr, Mo, and Tc have increased intensities at bottom of left lower the precipitate while Fe and Pd have a similar distribution in precipitate. Examining the phase diagram for Fe and Pd it appears that the Fe-Pd phase is forming as seen in the literature [26]. However, it would be difficult to identify the phases from the EDS intensity maps. From literature [59] the 5 metal precipitates can have multiple phases so it would not be unexpected that Cr, Mo and Tc are forming an additional phase. However, literature on a Cr, Mo and Tc phases was not found. In addition, there is the possibility that the Cr accumulated on the periphery after the precipitate was formed. However, as mentioned there does seem to overlap in the intensities of the Cr, Mo and Tc signals in the precipitate. It would appear the Ru and Rh have uniform distribution in the precipitate and are not forming any new phases. The Fe and Cr phases diagrams with Ru and Rh show there is some solubility in between Cr-Rh, Cr-Ru, Fe-Rh, and Fe-Ru which could be the reason that the Ru and Rh are uniformly distributed in the precipitate. This suggests that the use of the HT9 cladding interacting with the fuel is causing some microstructure and chemical changes in the 5 metal precipitates of the fuel. In addition, the EDS shows an enrichment of the Cr in the FCCI layer with possible Cs enrichment as well. The enrichment in the FCCI is an interesting phenomenon as the Fe does not exhibit enrichment in the FCCI layer while appearing in smaller precipitates in the fuel, whereas the Cr does not appear in the smaller precipitates. This enrichment of Cr is not completely unexpected: in out of pile corrosion tests of Fe-Cr alloys in simulated reactor conditions Cr has reacted to form Cr_2O_3, Cr_2Te_3 and other possible Cs-Cr-O phases [56]. Unfortunately, the region of the TEM foil containing the HT-9 cladding material broke off before analysis could be performed which limits this investigation to just the fuel side and FCCI. The Cr enrichment also corresponds to O enrichment in the FCCI as documented in Figures 9 and 10 which would suggest the formation of Cr_2O_3 in the FCCI which agrees with [26, 61]. Which would suggest that the FCCI is oxidative process and that there was the oxygen potential to form Cr oxides [26, 61, 64-66]. Unfortunately, the foil fractured before more detailed analysis could be performed in this region. The Te enrichments in the TEM foils do not correspond to any enrichment in Cr so it is unlikely that there was any formation of Cr_2Te_3 on the fuel side of the interface. The EDS of the TEM foils also indicate Te at the end of cracks and at the pores in the HBS structure of the MOX-MA fuel. Te is a volatile fission product that is a main component in the FCCI and degradation of the cladding [61-69]. While it was not possible to get quantitative information with EDS the results here correlate to the other research findings: a review of the literature indicates that volatile Te is migrating to the fuel clad interface and is part of the FCCI [61-69]. In the TEM EDS maps and foils there was no noticeable effects of the Am and Np additions to the MOX on the FCCI as compared with MOX without MA at similar burnups [53,54].

Conclusions

This research indicates that MA-MOX has the potential for being a transmutation fuel in a fast reactor spectrum. Throughout the observations reported in this work, there were no noticeable

changes to the fuel performance that could be attributed to the minor actinide additions. The observed fuel behavior is essentially MOX fuel behavior. Microstructural changes were observed with both optical and electron microscopy. The optical microscopy examination revealed that no central void had formed in the fuel and a HBS had formed in the periphery of the pellet. The electron microscopy confirmed these observations and in addition EBSD was performed of the center of the fuel that confirmed a subdivision of the grains had occurred. These techniques provide additional information about the microstructural development of the irradiated fuel and the diffusion of the cladding elements into the fuel. The TEM with EDS enabled the observation that Fe and Cr from the HT9 cladding had diffused into the 5 metal precipitates. It also elucidated that the precipitates were not a homogenous mixture of the Fe, Cr and the other 5 metals: instead that there was a heterogenous structure with possibly different phases present. In addition, the TEM investigation showed that Te was observed at the end of cracks in the FCCI zone. The combination of non-destructive and destructive testing techniques applied in combination with advanced electron microscopy provided new avenues to document the detailed characterization of irradiated fuels.

Acknowledgments

This work was supported by the U.S. Department of Energy, Advanced Fuels Campaign program in the Office of Nuclear Energy under DOE-NE Idaho Operations Office Contract DE-AC07-05ID14517. This manuscript was authored by a contractor for the U.S. Government. The publisher, by accepting the article for publication, acknowledges that the U.S. Government retains a nonexclusive, paid-up, irrevocable, worldwide license to publish or reproduce the published form of this manuscript, or allow others to do so, for U.S. Government purposes.

The authors would also like to acknowledge the staff at HFEF especially Paul Lind, Brian Frickey, and Korbin Traughber and the staff at EML

References

[1] J. Wallenius “Maximum efficiency nuclear waste transmutation” Annals Nucl. Energy 125 (2019) 74-79

[2] M. Atz, A. Salazar, F. Hirano, M. Fratoni, J. Ahn “ Assessment of the potential for criticality in the far field of a used nuclear fuel repository” Annals Nucl. Energy 124 (2019) 28-38

[3] P. Yang, Y. Wang, M.A. Rodriguez, P.V. Brady “Rock-welding materials development for deep borehole nuclear waste disposal” Mater. Chem. Phys. 221 (2019) 178-187

[4] B. Liu, K. Wang, J. Tu, F. Liu, L. Huang, W. Hu “ Transmutation of minor actinides in the pressure water reactors” Annals Nucl. Energy 64 (2014) 86-92

[5] B. Lui, R. Jia, R. Han, X. Lyu, J. Han, W. Li “Minor actinide transmutation characteristics in AP1000” Annals Nucl. Energy 115 (2018) 116-123

[6] W. Hu, J. Jing, J. Bi, C. Zhao, B. Liu, X. Ouyang “Minor actinides transmutation on pressurized water reactor burnable poison rods” Annals Nucl. Energy 110 (2017) 222-229

[7] R. Parrish, A. Aitkaliyeva “A review of microstructural features in fast reactor mixed oxide fuels” J. Nucl. Mater. 510 (2018) 644-660

[8] T. Kooyman, L. Buiron, G. Rimpault “Analysis of the impacts of homogeneous minor actinides loading in low void effect sodium fast reactor cores” Annals Nucl. Energy 124 (2019) 572-578

[9] N.V. Ivanov, Yu.A. Kazansky, G.V. Karpovich “The results of the transmutation of fission fragments in the spectrum of neutrons of thermal and fast reactors” Nucl. Energy Tech. 3 (2017) 220-223

[10] B.G. Hong, S.Y. Moon “Transmutation characteristics of minor actinides in low aspect ratio tokamak fusion reactor” Fus. Eng. Design 89 (2014) 2523-2528

[11] C. Yang, L. Cao, H. Wu, Y. Zheng, T. Zu “Neutronics analysis of minor actinides transmutation in a fusion-driven subcritical system” Fusion Eng. Des. 88 (2013) 2777-2784

[12] Y. Furudate, H. Shishido, N. Yusa, H. Hashizume “Construction of minor actinides reduction scenario in Japan utilizing fusion reactors” Prog. Nucl. Energy 103 (2018) 28-32

[13]A.A. Al Qaaod, H. Shahbunder, R.M. Refeat, E.A. Amin, S.U. EL-Kameesy “Transmutation performance of uniform and nonuniform distributions of plutonium and minor actinides in TRIGA Mark II ADS reactor” Annals Nucl. Energy 121 (2018) 101-107

[14] W. Uyttenhove, V. Sobolev, W. Maschek “Optimization of composite metallic fuel of minor actinide transmutation in an accelerator-driven system” J. Nucl. Mater. 416 (2011) 192-199

[15] S. Zhou, H. Wu, Y. Zheng “Flexibility of ADS for minor actinides transmutation in different two-stage PWR-ADS fuel cycle scenarios” Annals Nucl. Energy 111 (2018) 271-279

[16] F. Lebreton, D. Prieur, D. Horlait, T. Delahaye, A. Jankowiak, C. Leoriet, F. Jorion, E. Gavilan, F. Desmouliere “Recent progress on minor-actinide-bearing oxide fuel fabrication at CEA Marcoule” J. Nucl. Mater. 438 (2013) 99-107

[17] J. Wallenius, S. Bortot “A small lead-cooled reactor with improved AM-burning and non-proliferation characteristics” Annals Nucl. Energy 122 (2018) 193-200

[18] F. Gabrielli, A. Rineiski, B. Vezzoni, W. Maschek, C. Fazio, M. Salvatores “ASTRID-like Fast Reactor Cores for Burning Plutonium and Minor Actinides” Energy Procedia 71 (2015) 130-139

[19] B. Vezzoni, F. Gabrielli, A. Rineiski, A. Schwenk-Ferrero, V. Romanello, W. Maschek, C. Fazio, M. Salvatores “Plutonium and Minor Actinides incineration option using innovative Na-cooled fast reactors: Impacting on phasing-out and on-going fuel cycles” Prog. Nucl. Energy 82 (2015) 58-63

[20] P. Medvedev, S. Hayes, S. Bays, S. Novascone, L. Capriotti “Testing fast reactor fuels in a thermal reactor” Nucl. Eng. Des. 328 (2018) 154-160

[21] H.J. MacLean “Irradiation of AFC-2C and -2D Oxide Fuels for Actinide Transmutation in the ATR” INL/EXT-08-14252 (2008)

[22] H.A. Abderrahim, D.D. Bruyn, G. Van den Eynde, R. Fernandez, “Accelerator Driven Subcritical Systems” Encyclopedia of Nuclear Energy (2021) 191-202

[23] J.M. Harp “Baseline Postirradiation Examination of Fuel Rodlets from the AFC-2D Experiment” INL/MIS-17-42675

[24] K. Maeda, S. Sasaki, M. Kato, Y. Kihara “Radial redistribution of actinides in irradiated FR-MOX fuels” J. Nucl. Mater. 389 (2009) 78-84

[25] K. Maeda, K. Katsuyama, Y. Ikusawa, S. Maeda “Short-term irradiation behavior of low-density americium-doped uranium-plutonium mixed oxide fuels irradiated in a fast reactor” J. Nucl. Mater. 416 (2011) 158-165

[26] F. Cappia, B.D. Miller, J.A. Aguiar, L. He, D.J. Murray, B.J. Frickey, J.D. Stanek, J.M. Harp “Electron microscopy characterization of fast reactor MOX Joint Oxyde-Gaine (JOG)” J. Nucl. Mater. 531 (2020) 151964

[27] F. Cappia, K. Tanaka, M. Kato, K. McClellan, J. Harp “ Post-irradiation examinations of annular mixed oxide fuels with average burnup 4 and 5 % FIMA” J. Nucl. Mater. 533 (2020) 152076

[28] R.J. Parrish, F. Cappia, A. Aitkaliyeva “Comparison of the radial effects of burnup on fast reactor MOX fuel microstructure and solid fission products” J. Nucl. Mater. 531 (2020) 152003

[29] M. Teague, B. Gorman, B. Miller, J. King “EBSD and TEM characterization of high burn-up mixed oxide fuel” J. Nucl. Mater. 444 (2014) 475-480

[30] M. Pelletier, Y. Guerin, “2.03- Fuel Performance of Fast Spectrum Oxide Fuel” Compr.

Nucl. Mater., Elsevier (2020) pp 72-105

[31] D.C. Crawford, D.L. Porter, S.L. Hayes, Fuels for sodium-cooled fast reactors: US perspective, J. Nucl. Mater. 371 (2007) 202–231. Doi:https://doi.org/10.1016/j.jnucmat.2007.05.010.

[32] T. Nagata, H. Yamashita, A Review of Fast Reactor Program in Japan, in: 34th Annu. Meet. Tech. Work. Gr. Fast React., Almaty/Kurchatov, Republic of Kazakhstan, 2001: pp. 293–312.

[33] M. Teague, B. Gorman, J. King, D. Porter, S. Hayes, Microstructural characterization of high burn-up mixed oxide fast reactor fuel, J. Nucl. Mater. (2013). doi:10.1016/j.jnucmat.2013.05.067.

[34] M. Naganuma, S. Koyama, T. Asaga, J. Noirot, D. Lespiaux, J. Rouault, G. Crittenden, C. Brown " High Burnup irradaition performance of annular fuel pins irradaited in fast reactor PFR" International symposium on MOX fuel cycle technologies for medium and long term deployment; Vienna (Austria); 17-21 May 1999

[35] C.T. Walker, G. Nicolaou, Transmutation of neptunium and americium in a fast neutron flux: EPMA results and KORIGEN predictions for the superfact fuels, J. Nucl. Mater. 218 (1995) 129–138. doi:https://doi.org/10.1016/0022-3115(94)00649-0.

[36] C. Prunier, F. Boussard, L. Koch, M. Coquerelle, Some Specific Aspects of Homogeneous Americium-and Neptunium-Based Fuels Transmutation Through the Outcomes of the Superfact Experiment in Phénix Fast Reactor, Nucl. Technol. 119 (1997) 141–148. doi:10.13182/NT97-A35382.

[37] K. Tanaka, S. Miwa, I. Sato, T. Hirosawa, H. Obayashi, S.-I Koyama, H. Yoshimochi, K. Tanaka "Microstructure and elemental distribution of americium-containing uranium plutonium mixed oxide fuel under a short-term irradiation test in a fast reactor" J. Nucl. Mater. 385 (2009) 407-412

[38] K. Tanaka, S. Miwa, S.I. Sekine, H. Yoshimochi, H. Obayashi, S.I. Koyama "Restructuring and redistribution of actinides in Am-MOX fuel during the first 24 h of irradiation" J. Nucl. Mater. 440 (2013) 480-488

[39] K. Tanaka, S. Miwa, S. Sekine, H. Yoshimochi, H. Obayashi, S. Koyama, Restructuring and redistribution of actinides in Am-MOX fuel during the first 24h of irradiation, J. Nucl. Mater. 440 (2013) 480–488. doi:https://doi.org/10.1016/j.jnucmat.2013.01.351.

[40] T. Delahaye, F. Lebreton, D. Horlait, N. Herlet, P. Dehaudt "Application of the UMACS process to highly dense $U_{1-x}Am_xO_{2\pm\delta}$ MABB fuel fabrication for the DIAMINO irradiation" J. Nucl. Mater. 432 (2013) 305-312

[41] S. Bejaoui T. Helfer, S. Bendotti, T. Lambert "Description and thermal simulation of the DIAMINO irradiation experiment of transmutation fuel in the OSIRIS reactor" Prog. Nucl. Ener. 113 (2019) 28-44

[42] E. D'Agata, P.R. Hania, S. Bejaoui, C. Sciolla, T. Wyatt, M.H.C. Hannink, N. Herlet, A. Jankowiak, F.C. Klaassen, J.-M. Lapetite, D.A. Boomstra, M. Phelip, F. Delage "The results of the irradiation experiment MARIOS on americium transmutation" Ann. Nucl. Ener. 62 (2013) 40-49

[43] E. D'Agata, P.R. Hania, J. McGinley, J. Somers, C. Sciolla, P.J. Baas, S. Kamer, R.A.F. Okel, I. Bobeldijk, F. Delage, S. Bejaoui "SPHERE: Irradiation of sphere-pac fuel of $UPuO_{2-x}$ containing 3% Americium" 275 Nucl. Eng. Des. (2014) 300-311

[44] T. Kooyman "Current start of partitioning and transmutation studies for advanced nuclear fuel cycles" Annals Nucl. Ener. 157 (2021) 108239

[45] R.E. Mason, S.P. Willson, H.W. Majors, D.E.R Martinez, J.T. Dunwoody, K.J. McClellan, D.D. Byler "AFC2-C/D Fuel Pellet Data Package" LA-UR-08-03727

[46] Jason M. Harp, Steven L. Hayes, Pavel G. Medvedev, Douglas L. Porter, Luca Capriotti "Testing Fast Reactor Fuels in a Thermal Reactor: A Comparison Report" NTRD-FUEL-2017-000148

[47] M. Teague, M. Tonks, S. Novascone, S. Hayes, Microstructural modeling of thermal conductivity of high burn-up mixed oxide fuel, J. Nucl. Mater. 444 (2014) 161–169. doi:https://doi.org/10.1016/j.jnucmat.2013.09.035

[48] A.E. Craft, D.M. Wachs, M.A. Okuniewski, D.L. Chichester, W.J. Williams, G.C. Papaioannou, A.T. Smolinski, Neutron Radiography of Irradiated Nuclear Fuel at Idaho National Laboratory, Phys. Procedia. 69 (2015) 483–490. doi:10.1016/J.PHPRO.2015.07.068.

[49] W.J. Maeck, R.P. Larsen, J.E. Rein "Burnup Determination for Fast Reactor Fuels: A Review and Status of the Nuclear Data and Analytical Chemistry Methodology Requirements" NTIS Report TID 26209. 1973

[50] J.M. Harp, P.A. Demkowicz, P.L. Winston, J.W. Sterbentz, "An analysis of nuclear fuel burnup in the AGR-1 TRISO fuel experiment using gamma spectrometry, mass spectrometry, and computational simulation techniques" Nucl. Eng. Des. 278 395-405 (2014)

[51] H. Matzke, On the rim effect in high burnup UO_2 LWR fuels, J. Nucl. Mater. 189 (1992) 141–148.

[52] T.J. Gerczak, C.M. Parish, P.D. Edmondson, C.A. Baldwin, K.A. Terrani "Restructuring in high burnup UO_2 studied using modern electron microscopy" J. Nucl. Mater. 509 (2018) 245-259

[53] G. Khvostov "Modeling of central void formation in LWR fuel pellets due to high-temperature restructuring" Nucl. Eng. Tech. 50 (2018) 1190-1197

[54] S. Novascone, P. Medvedev, J.W. Peterson, Y. Zhang, J. Hales "Modeling porosity migration in LWR and fast reactor MOX fuel using the finite element method" J. Nucl. Mater. 508 (2018) 226-236

[55] V.V. Rondinella, T. Wiss “The high burn-up structure in nuclear fuel” Materials Today 13 (2010) 24-32

[56] M. Teague, B. Gorman, J. King, D. Porter, S. Hayes “Microstructural characterization of high burn-up mixed oxide fast reactor fuel” J. Nucl. Mater. 441 (2013) 267-273

[57] F. Cappia, D. Pizzocri, M. Marchetti, A. Schubert, P. Van Uffelen, L. Luzzi, D. Papaioannou, R. Macian-Juan, V.V. Rondinella “Microhardness and Young’s modulus of high burn-up UO_2 fuel” J. Nucl. Mater. 479 (2016) 447-454

[58] J. Noirot, L. Desgranges, J. Lamontagne “Detailed characterizations of high burn-up structures in oxide fuels. Journal of Nuclear Materials 372: 318-33

[59] J. Noirot, I. Zacharie-Auburn, T. Blay “Focused ion beam-scanning electron microscope examination of high burn-up UO_2 in the center of a pellet” Nucl. Eng. Tech 50 (2018) 259-267

[60] K. Maeda, K. Tanaka, T. Asaga, H. Furuya “Distributions of volatile fission products in or near the fuel-cladding of the FBR MOX fuel pins irradiated to high burn-up” J. Nucl. Mater. 344 (2005) 274-280

[61] K. Maeda, T. Asaga, “Change of fuel-to-cladding gap width with the burn-up in FBR MOX fuel irradiated to high burn-up” J. Nucl. Mater. 327 (2004) 1-10

[62] R.J. Parrish, K.E. Wright, A.J. Winston, C. McKinney, J.M. Harp, A. Aitkaliyeva “Characterization of solid fission products in 13.7% FIMA MOX fuel using electron microscopy techniques” J. Nucl. Mater. 524 (2019) 67-79

[63] R. Parrish, A. Winston, J. Harp, A. Aitkaliyeva “TEM characterization of high burnup fast reactor MOX fuel” J. Nucl. Mater. 527 (2019) 151794

[64] S. Ukai, Y. Yamazaki, N. Oono, S. Hayashi, “Corrosion behavior of 9CrODS steel by simulated fission product cesium and tellurium” J. Nucl. Mater. 440 (2013) 39-45

[65] F. De Keroulas, R. Le Beuze, D. Calais, A. van Craeynest, M. Conte, Reaction a l'interface gaine (acier inoxydable) combustible (oxyde mixte (UPu)O2±x) dans les elements combustibles irradies, Journal of Nuclear Materials 43: 313-320, 1972

[66] C.E. Johnson, C.E. Crouthamel, Cladding interactions in mixed oxide irradiated fuels, Journal of Nuclear Materials 34: 101-104, 1970

[67] M. Aubert, D. Calais, R. Le Beuze, Role de l'iodure de cesium sur le developpement des reactions combustible-gaine, Journal of Nuclear Materials 60: 279-290, 1976

[68] M.G. Adamson, E.A. Aitken “On the CsTe Fission Product-Induced attach and embrittlement of stainless steel cladding in oxide fuel pins” J. Nucl. Mater. 132 (1985) 160-166

[69] K. Sasaki, T. Tanigaki, R. Fujimura, K. Fukumoto, M. Uno “The corrosion product of Cs-Te corrosive compound with 11Cr-Ferritic Martensitic Steel and 9Cr-Oxide Dispersion strengthened steel” J. Nucl. Mater. 460 (2015) 107-113

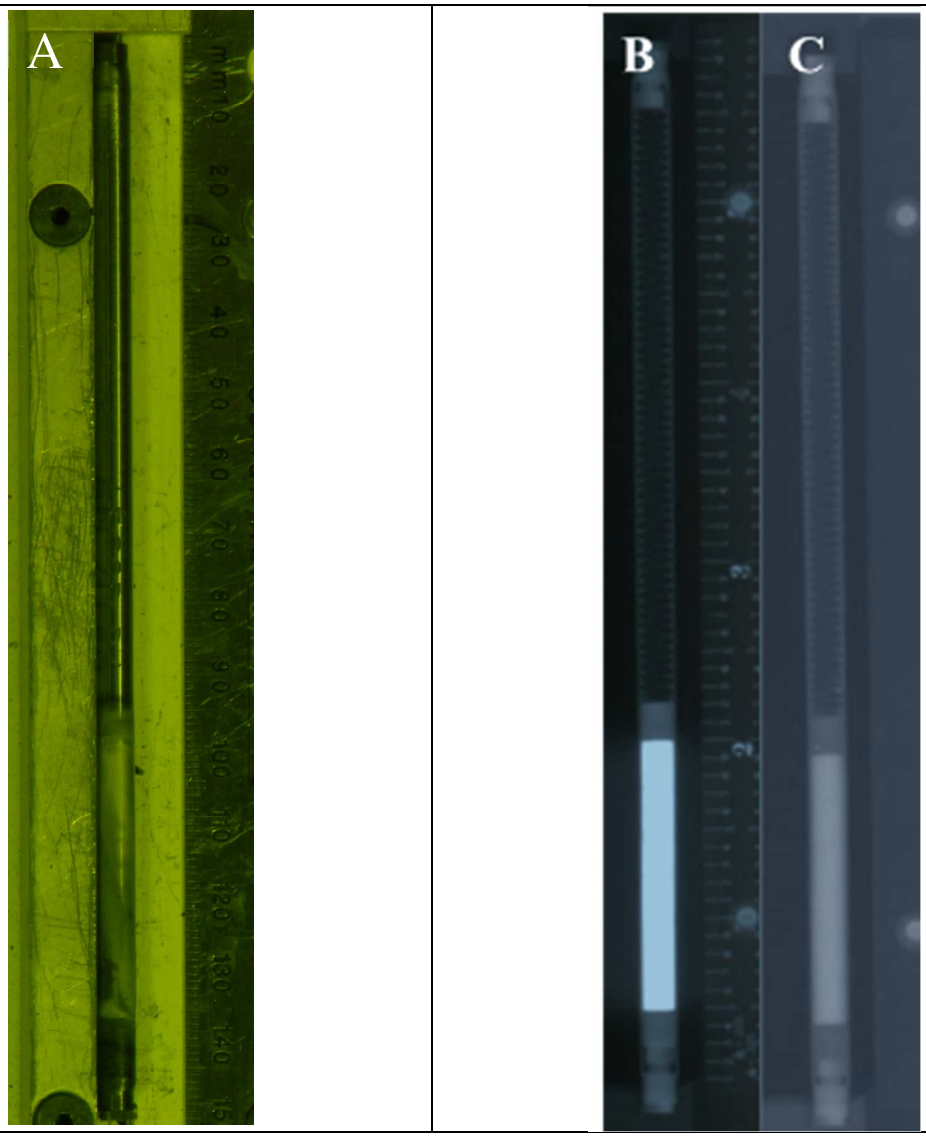

Figure 1: A) Visual examination B) Thermal neutron radiography C) Epithermal neutron radiography of the rodlet.

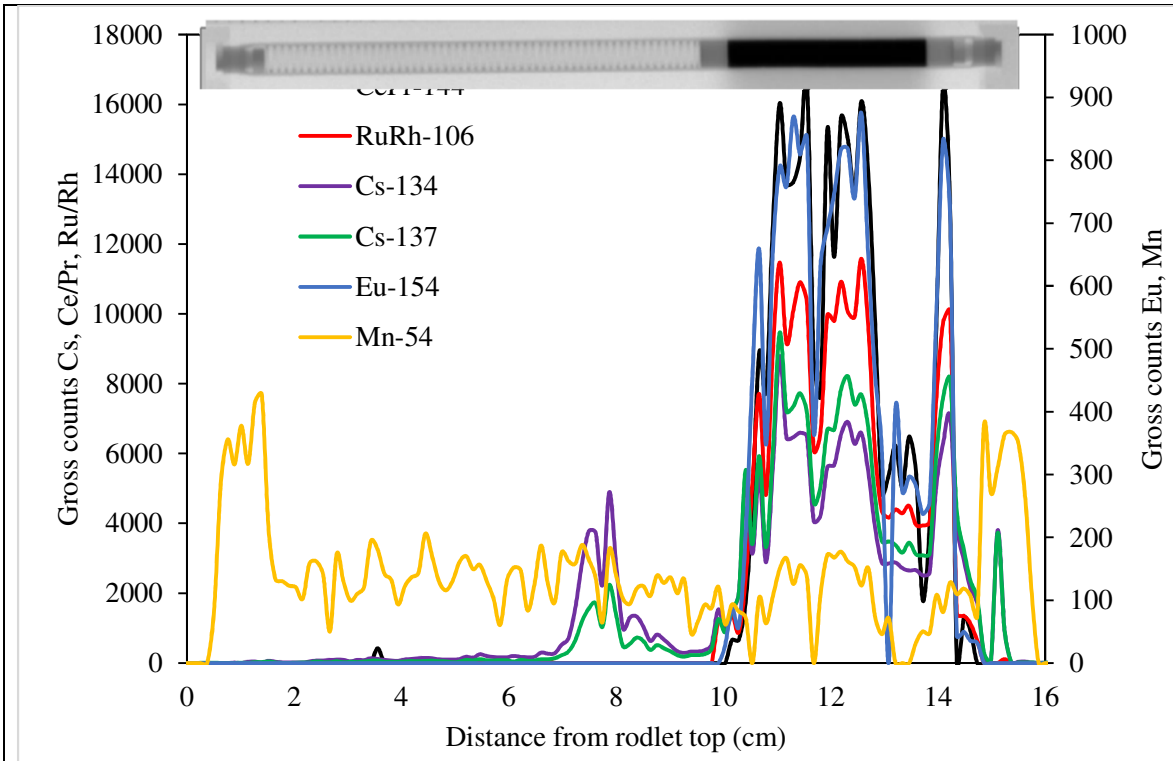

Figure 2: Axial gamma spectroscopy of the rodlet. At the top of the figure a high-contrast version of the neutron radiography image shown in Figure 1B is included to show the position of the active fuel stack (in black). The small peak of Ce around 3-4 cm is believed to be anomaly in the measurement. The decrease in the signal of all of the elements between 13-14 cm is not understood by the authors.

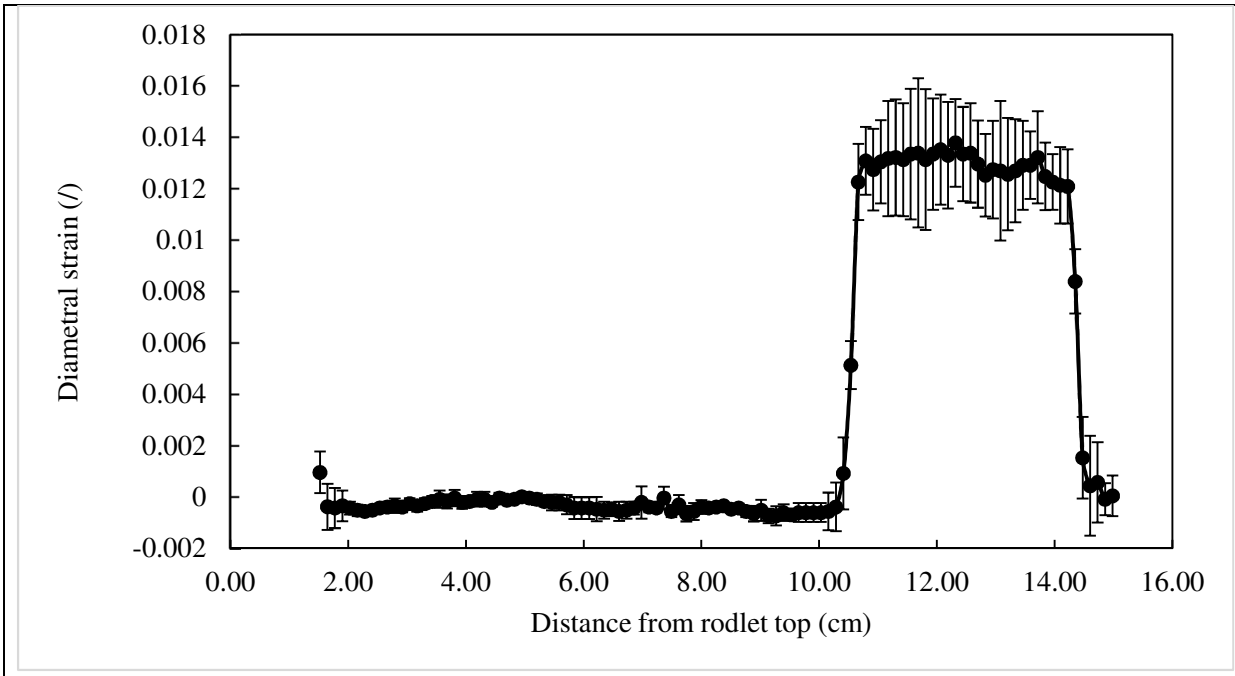

Figure 3: Axial profile of the cladding diametral strain of the rodlet.

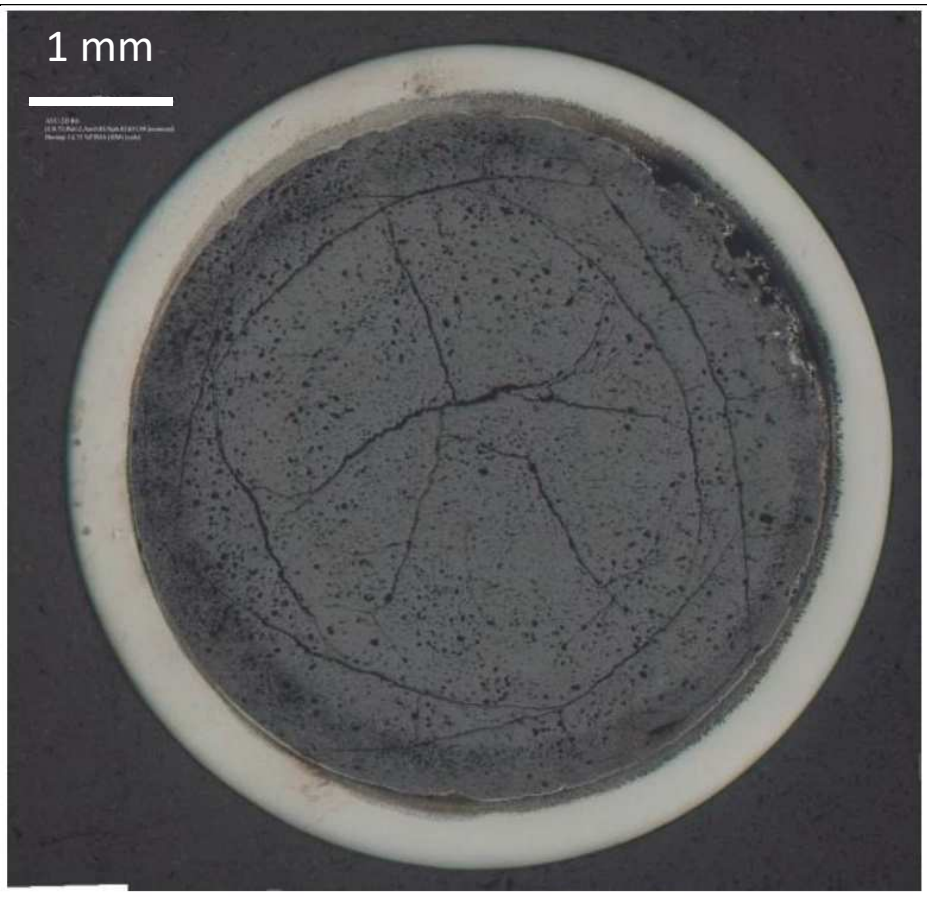

Figure 4: Optical image montage (50X) of the fuel cross section.

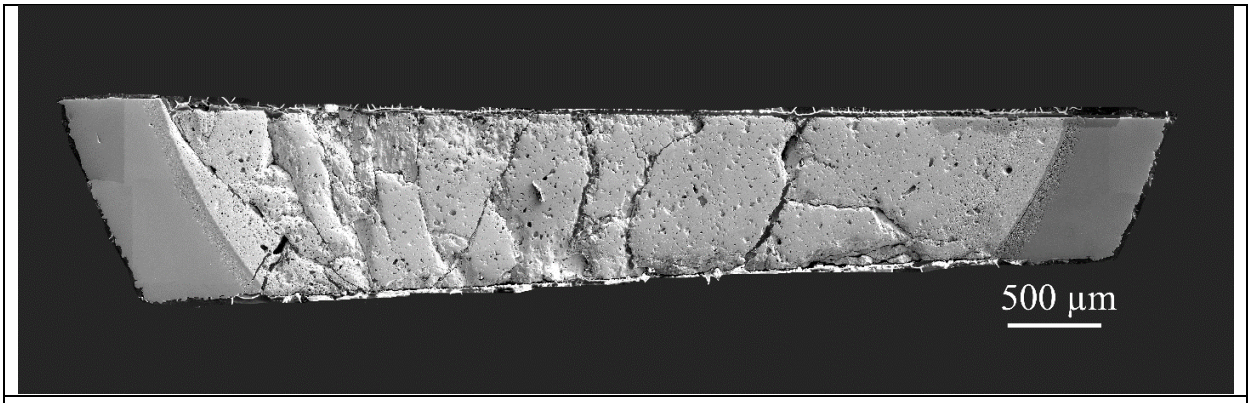

(a)

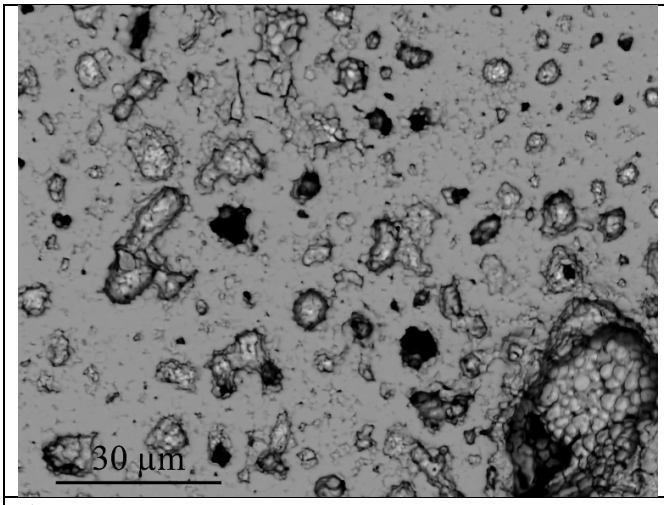

(b)

Figure 5: (a) SE SEM overview of the MA-MOX sample. (b) High magnification BSE image showing the microstructure at the pellet periphery. The typical features characterize the HBS are visible micrometric pores with faceted surface distributed within the sub-micrometric grains.

Figure 6: The EBSD of the near center region of the pellet. The internal restructuring of the fuel can be observed. The dark spots and corresponding areas of random index patterns are pores in the material. A) Is the IPF with low angle grain boundaries (2-15 °) marked in the image. The black circles highlight the regions of subdivision. B) The IPF and without the low angle grain boundaries marked. C) The image quality.

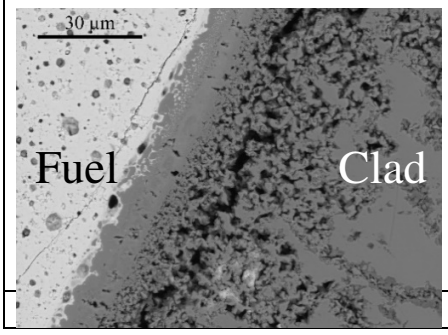

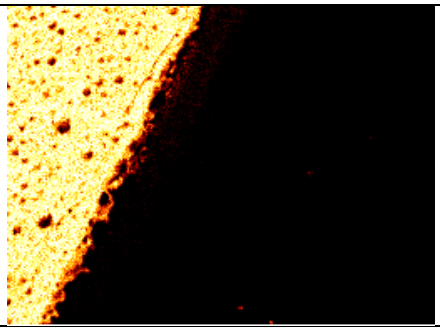

(b) Uranium

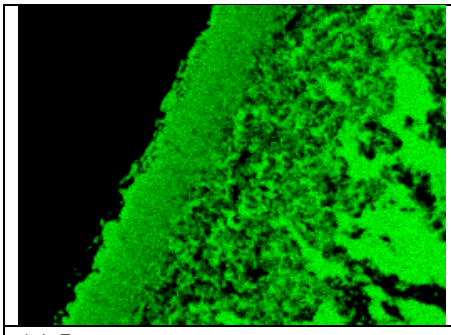

(c) Iron

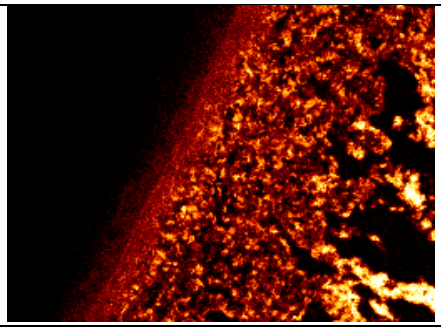

(d) Chromium

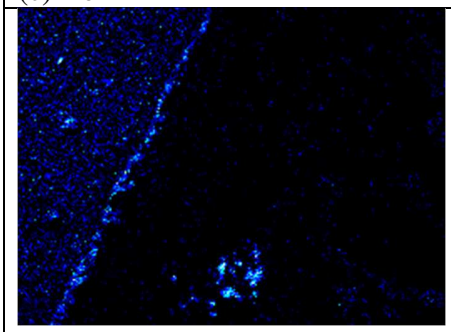

(e) Cesium

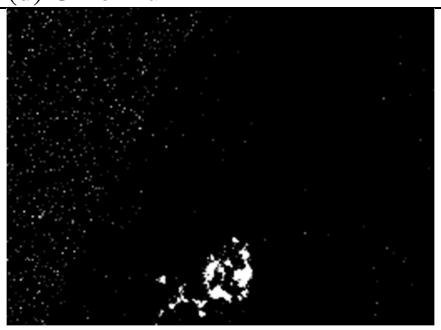

(f) Tellurium

Figure 7: (a) BSE image of the FCCI region. EDS qualitative maps of (b) U, (c) Fe, (d) Cr, (e) Cs, (f) Te.

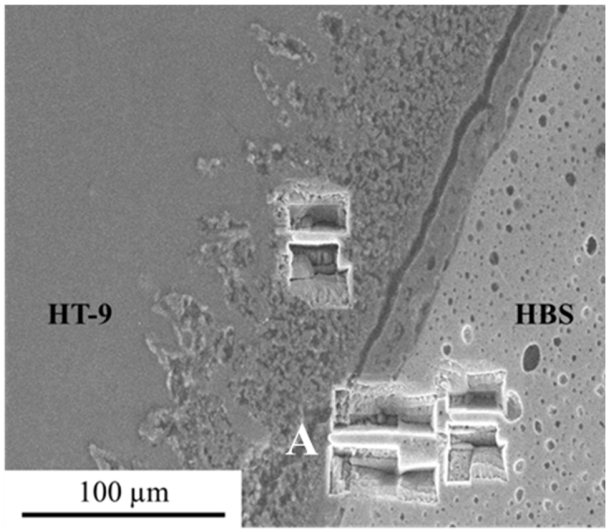

Figure 8: SEM image of MA-MOX fuel. The FCCI zone and the location of the TEM foils extracted for analysis of the samples..

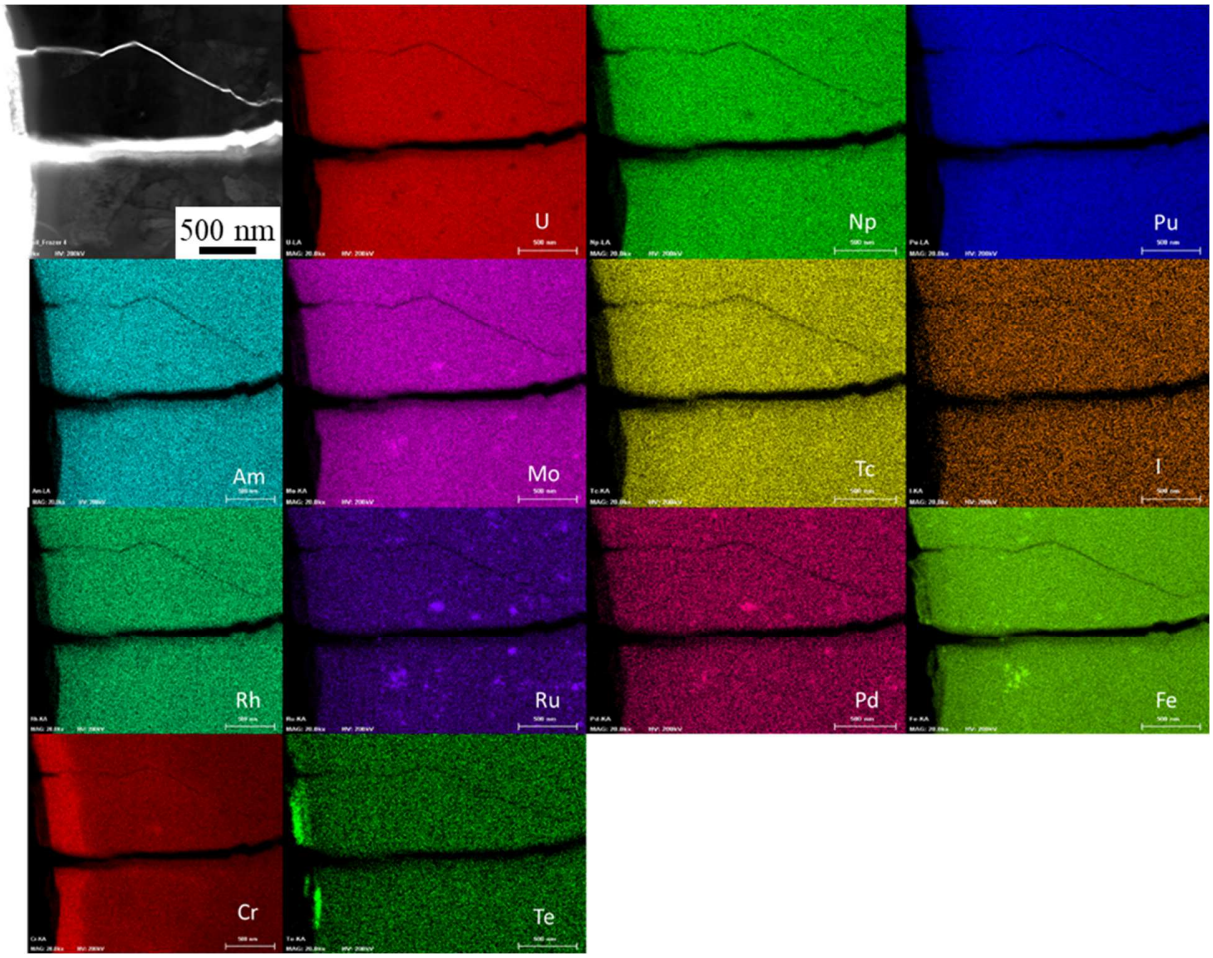

Figure 9: The EDS maps form TEM foil A in Figure 6. These are intensity maps are at the FCCI/Fuel boundary. The maps show an enrichment of Cr in the FCCI layer and Te enrichments at the end of cracks in the fuel. In addition, Fe in small precipitates can be observed.

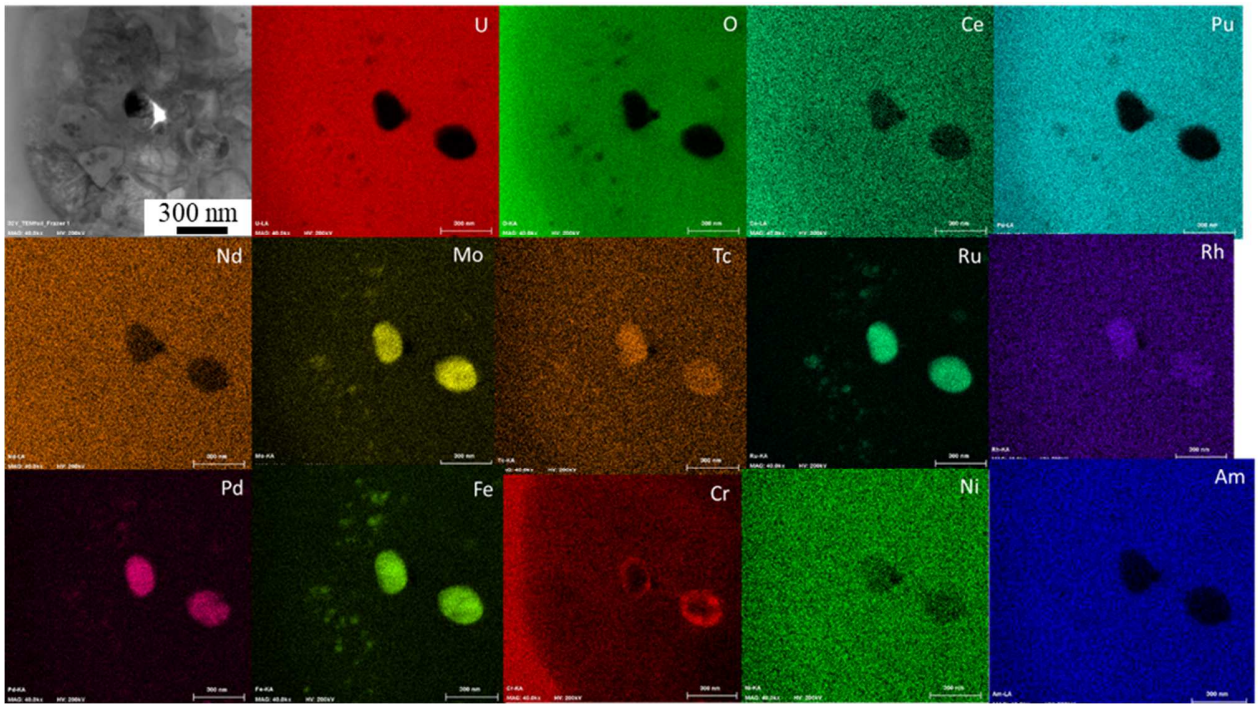

Figure 10: The EDS maps form TEM foil A in Figure 8. These are intensity maps in the fuel near the FCCI/Fuel boundary. EDS of two large precipitates and several smaller precipitates in the fuel. There is some heterogeneity in the elements of the 5 metal precipitates. Also, the enrichment of Cr and O in the FCCI layer can be observed.

Table 1: Rodlet nominal parameters and irradiation data.

Fuel nominal composition	$(U_{0.75}Pu_{0.20}Am_{0.03}Np_{0.02})O_{1.986}$
Cladding material	HT-9
Fuel nominal diameter (mm)	4.86
Cladding nominal outer diameter (mm)	5.84
Initial gap (mm)	0.05
Average Linear Heat Generation Rate (LHGR) (W/cm)	243
Initial Porosity Range (%)	7.5

Table 2: Fission gas release data

Plenum pressure (MPa)	Kr and Xe release (%)	Gas Composition (%)					
		He	N	O	Ar	Kr	Xe
1.25	56.8	36.1	2.7	0.6	0.3	6.9	52.8